Experimental study of the electronic density of states in aluminium-based intermetallics

2005 J. Phys.: Condens. Matter 17 6911

(http://iopscience.iop.org/0953-8984/17/43/010)

INSTITUTE OF PHYSICS PUBLISHING JOURNAL OF PHYSICS: CONDENSED MATTER

J. Phys.: Condens. Matter **17** (2005) 6911–6924 doi:10.1088/0953-8984/17/43/010

Experimental study of the electronic density of states in aluminium-based intermetallics

E Belin-Ferré[1], M Klanjšek[2], Z Jagličić[3], J Dolinšek[2] and J M Dubois[4]

[1] Laboratoire de Chimie Physique Matière et Rayonnement, Université Pierre et Marie Curie (UMR 7614 CNRS), 11 rue Pierre et Marie Curie, F-75231 Paris cedex 05, France
[2] J Stefan Institute, University of Ljubljana, Jamova 39, SI-1000 Ljubljana, Slovenia
[3] Institute of Mathematics, Physics and Mechanics, Jadranska 19, SI-1000 Ljubljana, Slovenia
[4] Institut Jean Lamour (FR 2797 CNRS-INPL-UHP)—LSG2M—Ecole des Mines, Parc de Saurupt, F-54042 Nancy cedex, France

Received 17 June 2005, in final form 28 July 2005
Published 14 October 2005
Online at stacks.iop.org/JPhysCM/17/6911

Abstract

We report on an experimental investigation of the electronic density of states (DOS) in aluminium-based intermetallics by three experimental techniques: electrical resistivity, NMR spin–lattice relaxation and soft x-ray emission spectroscopy (SXES). The investigated samples were alloys of Al with transition elements Cu, Fe, Cr, Pd and Mn and sometimes also a small amount of B. The samples were structurally very different and included (1) regular periodic intermetallic compounds, (2) large-unit-cell intermetallics that are translationally periodic on the scale of several nanometres and exhibit local polytetrahedral order (like quasicrystals) on the scale of interatomic distances and (3) quasicrystals. Correlation analysis between the DOS parameters determined independently by the three techniques employed showed that the order of samples with decreasing metallic character was the same in all experiments. Quantitative evaluation of the DOS at E_F has shown that in regular alloys the DOS is reduced to about 50% of the free-electron-like value in fcc Al metal, whereas the reduction becomes increasingly larger on going to large-unit-cell periodic solids and quasicrystals. Our results also demonstrate that low resistivities are accompanied by positive temperature coefficient (PTC) variation, whereas samples with large resistivity exhibit negative temperature coefficient (NTC). Samples with a resistivity of about 200 $\mu\Omega$ cm appear to be at a crossover from PTC to NTC resistivity, resulting in a temperature-compensated resistivity with essentially zero temperature coefficient. Magnetic properties of the samples are also presented.

1. Introduction

Physical properties of materials with metallic character like electrical conductivity, electronic contribution to the thermal conductivity, Pauli paramagnetic susceptibility and thermoelectric

power are related to the density of states (DOS) of conduction electrons at the Fermi energy E_F. In addition, the electronic DOS is considered to have influence also on surface properties of the material, such as wetting of oxidized metallic surfaces by polar liquids like water, where electrostatic forces between water molecules and the electronic cloud within the bulk material are considered to affect the contact angle of a water droplet on the surface [1]. In free-electron-like metals and alloys, the DOS at E_F is usually large and does not exhibit pronounced variation with energy in the vicinity of the Fermi level over an energy interval of the order $k_B T$. In quasicrystals (QCs) [2], the quasiperiodic arrangement of atoms strongly reduces the DOS and introduces a pseudogap in the vicinity of E_F. Consequently, electronic transport phenomena of QCs are reduced with respect to regular metals and alloys. There exist several experimental methods to determine the electronic DOS of a solid system. Electrical conductivity σ is related to the total DOS at the Fermi level, $g(E_F)$; nuclear magnetic resonance (NMR) spin–lattice relaxation rate T_1^{-1} due to nuclear spin relaxation via conduction electrons depends quadratically [3] on the DOS, $T_1^{-1} \propto g^2(E_F)$, whereas soft x-ray emission spectroscopy [4] (SXES) supplies information on the energy distribution of selected partial densities of occupied states around a chosen element in a solid.

In the last two decades, ternary, quaternary and pentary intermetallic compounds became of high interest. Many of these alloys exhibit complex phase diagrams, which at certain concentrations form simple intermetallic phases, whereas in some other concentration ranges exceptional intermetallic phases with large unit cells, comprising several hundred up to some thousand atoms, can be found. In addition, quasicrystalline phases with quasiperiodic atomic order that exhibits crystallographically 'forbidden' symmetries (icosahedral, decagonal etc) are sometimes present in the phase diagram. Emblematic examples of such systems are Al–Cu–Fe and Al–Pd–Mn families of intermetallics. Electronic transport properties of compounds from the same family can be markedly different, ranging from typical metallic in simple compounds to semimetallic-to-insulating-like in QCs. Many families belonging to this class of intermetallics are aluminium rich and contain other transition elements, like Cu, Mn, Fe, Cr and Pd, in substantial concentrations. The aim of this paper is twofold: (i) to get insight into the variation of the electronic DOS between compounds with different types of structural order (i.e. between simple periodic compounds, large-unit-cell compounds and QCs) and (ii) to compare the DOS information obtained independently by three experimental techniques, the electrical resistivity, the NMR relaxation and the soft x-ray emission spectroscopy. For that purpose we determined the electronic DOS on a selected set of 11 Al-based samples by the three above-mentioned techniques and made a correlation analysis. In the paper we describe first the set of samples pertinent to this study. Next we analyse their magnetic properties and present the DOS determination. The data are finally discussed in the last section.

2. Sample selection and characterization

The investigated set of materials included 11 samples, comprising icosahedral QCs, samples with decagonal order, large-unit-cell intermetallics recognized as quasicrystalline approximants and regular periodic intermetallic compounds. Six samples were sintered-powder polycrystals, whereas five were monocrystals, grown by either Czochralski or Bridgman techniques. The compositional and structural data were obtained from characterization by x-ray diffraction (XRD) and scanning electron microscope (SEM) techniques. Backscattered electron (BSE) images were used to check for the presence of secondary phases, whereas energy-dispersive x-ray spectroscopy (EDXS) was employed to determine the chemical composition. The sintered-powder samples generally contained small amounts of precipitates of a secondary phase and micro- and nanoscale porosity at the grain

Table 1. Sample characterization data.

Number	Composition	Abbreviation	Structural data	Production technique
1	$Al_{59.5}Cu_{25.3}Fe_{12.2}B_3$	*i*-AlCuFeB-3	Polycrystal; icosahedral + Fe_2AlB_2 precipitates	Sintered powder
2	$Al_{61.5}Cu_{25.3}Fe_{12.2}B_1$	*i*-AlCuFeB-1	Polycrystal; icosahedral + Fe_2AlB_2 precipitates	Sintered powder
3	$Al_{69.8}Pd_{21.8}Mn_{8.4}$	*i*-AlPdMn-n	Monocrystal; icosahedral (not annealed)	Czochralski
4	$Al_{70}Pd_{22.1}Mn_{7.9}$	*i*-AlPdMn-a	Monocrystal; icosahedral (annealed)	Czochralski
5	$Al_{70}Cu_9Cr_{10.5}Fe_{10.5}$	AlCuCrFe	Polycrystal; O_1-orthorhombic approximant of decagonal phase	Sintered powder
6	$Al_{77.5}Cr_{16.5}Fe_6$	AlCrFe	Polycrystal; O_1-orthorhombic approximant of decagonal phase + traces of monoclinic $Al_{13}Fe_4$	Sintered powder
7	$Al_{72.9}Pd_{22.9}Mn_{4.2}$	Ψ-AlPdMn	Monocrystal; Ψ-phase (orthorhombic)	Bridgman
8	$Al_{73}Pd_{22.9}Mn_{4.1}$	ξ'-AlPdMn-1	Monocrystal; ξ'-phase (orthorhombic)	Bridgman
9	$Al_{72.7}Pd_{23.2}Mn_{4.1}$	ξ'-AlPdMn-2	Monocrystal; ξ'-phase (orthorhombic)	Bridgman
10	$Al_{70}Cu_{20}Fe_{10}$	ω-AlCuFe	Polycrystal; ω-phase (tetragonal)	Sintered powder
11	$Al_{41.8}Cu_{57.2}B_1$	AlCuB	Polycrystal; orthorhombic Al_3Cu_4 + cubic Cu_9Al_4 + traces of AlB_2	Sintered powder

boundaries, as typical for this kind of sample-preparation technique. The monocrystalline samples were single-phase materials with no measurable contamination with secondary phases. The order in which the samples appear in the description below coincides with the decreasing electrical resistivity of the samples, to be presented in the following. A summary of the compositional and structural information on the samples is also given in table 1.

Sample (1) was a polycrystalline icosahedral $Al_{59.5}Cu_{25.3}Fe_{12.2}B_3$ QC (in the following abbreviated as *i*-AlCuFeB-3), which contained precipitates of a ferromagnetic Fe_2AlB_2 compound, identified previously by Brien *et al* [5]. Sample (2) was a polycrystalline icosahedral $Al_{61.5}Cu_{25.3}Fe_{12.2}B_1$ QC (*i*-AlCuFeB-1), also containing ferromagnetic Fe_2AlB_2 precipitates. Sample (3) was a Czochralski-grown monocrystalline icosahedral $Al_{69.8}Pd_{21.8}Mn_{8.4}$ (*i*-AlPdMn-n) QC that was not annealed after synthesis, whereas sample (4) with composition $Al_{70}Pd_{22.1}Mn_{7.9}$ (*i*-AlPdMn-a) was cut from the same ingot and was annealed at 800 °C. Sample (5) was a polycrystalline material of nominal composition $Al_{70}Cu_9Cr_{10.5}Fe_{10.5}$ (AlCuCrFe). Its phase was an O_1-orthorhombic approximant of the decagonal phase [6]. Sample (6) was a polycrystalline material of nominal composition $Al_{77.5}Cr_{16.5}Fe_6$ (AlCrFe), consisting of the same O_1-orthorhombic approximant phase [7]

and some traces of monoclinic $Al_{13}Fe_4$. The following three samples were large-unit-cell orthorhombic compounds from the ξ'-Al–Pd–Mn family [8–11] of intermetallics, which are periodic approximants of the icosahedral *i*-Al–Pd–Mn QCs. The ξ'-Al–Pd–Mn family contains the basic ξ' phase with the orthorhombic unit cell ($a \approx 2.35$ nm, $b \approx 1.66$ nm and $c \approx 1.23$ nm), that comprises 320 atoms and a set of variant phases with the same a and b parameters, but increasingly larger c parameter, approximately of the ratio $1:(1+\tau):(2+\tau):(3+\tau)$, where τ is the golden mean. The phase with $c \approx 5.70$ nm is named the Ψ phase and contains about 1500 atoms in the unit cell. The local order in all phases of the ξ' family is based on the same structural unit—the pseudo-Mackay icosahedron—as that of the *i*-Al–Pd–Mn QCs. The samples were grown by the Bridgman technique and were single-phase monocrystalline materials, free of grain boundaries and secondary phases. Sample (7) was in the Ψ phase with the composition $Al_{72.9}Pd_{22.9}Mn_{4.2}$ (Ψ-AlPdMn), whereas the other two were in the ξ' phase: sample (8) had the composition $Al_{73}Pd_{22.9}Mn_{4.1}$ (ξ'-AlPdMn-1) and sample (9) $Al_{72.7}Pd_{23.2}Mn_{4.1}$ (ξ'-AlPdMn-2). Sample (10) was a tetragonal ω-phase polycrystalline material of composition $Al_{70}Cu_{20}Fe_{10}$ (ω-AlCuFe). The last sample (11) was a polycrystalline material of average composition $Al_{41.8}Cu_{57.2}B_1$ (AlCuB). Its majority phase was orthorhombic Al_3Cu_4 and the minority phase (at most 20%) was cubic Cu_9Al_4. Traces of AlB_2 were detected also. The samples ω-AlCuFe and AlCuB are referred in the following as 'regular alloys', as their structure does not show such high complexity as the large-unit-cell intermetallics and QCs.

The above 11 samples are all based on aluminium and contain transition elements Cu, Fe, Cr, Pd and Mn that incorporate into the lattice, whereas B is added in small quantities mainly for improving mechanical properties. Boron forms intermetallic compounds that appear as precipitates (isolated islands) in the host matrix of other elements.

3. Magnetic properties

Magnetic properties were investigated by measuring temperature-dependent magnetic susceptibility, $\chi(T)$, and the magnetization as a function of the magnetic field, $M(H)$. A Quantum Design SQUID magnetometer, equipped with a 5 T magnet, was used. The $\chi(T)$ experiments were performed in a temperature interval from 300 to 2 K in a magnetic field $H = 1$ kOe, except for the two ferromagnetic (FM) samples, where a lower field $H = 100$ Oe was employed. These fields were low enough that the $M(H)$ dependence was still linear, so that $\chi = M/H$ is analysed in the following.

The two boron-containing icosahedral QCs, *i*-AlCuFeB-3 and *i*-AlCuFeB-1, exhibit a typical FM transition at a temperature $T_C \approx 300$ K (figure 1(a)), which is the same for both samples. The $M(H)$ curves taken at 5 K (figure 1(b)) also show typical FM behaviour with saturated magnetization above $H \approx 10$ kOe. This ferromagnetism is not an intrinsic property of the *i*-Al–Cu–Fe icosahedral phase but occurs due to the Fe_2AlB_2 precipitates in the samples [5]. The saturated magnetization of the *i*-AlCuFeB-3 sample, calculated *per B atom*, is about three times larger than that of the *i*-AlCuFeB-1. When calculated in units *per B atom*, the saturated magnetizations of the two samples should be the same in the case where all B atoms are located in an FM environment. Since this is not the case, only a fraction of B atoms form the FM compound, the remaining boron being located in a non-FM environment.

The temperature-dependent susceptibilities of the other nine samples (shown in the group 'all others' in figure 1(a)) are displayed on an expanded vertical scale in figures 1(c), (d). Three of the samples (*i*-AlPdMn-n, AlCuCrFe and AlCrFe) exhibit pronounced Curie-paramagnetic $\chi \propto 1/T$ behaviour (figure 1(c)), indicating the presence of localized magnetic moments. These samples can be classified as paramagnets. The susceptibilities of the other six samples (figure 1(d)) exhibit very weak or no temperature dependence, apart from the trivial tiny Curie

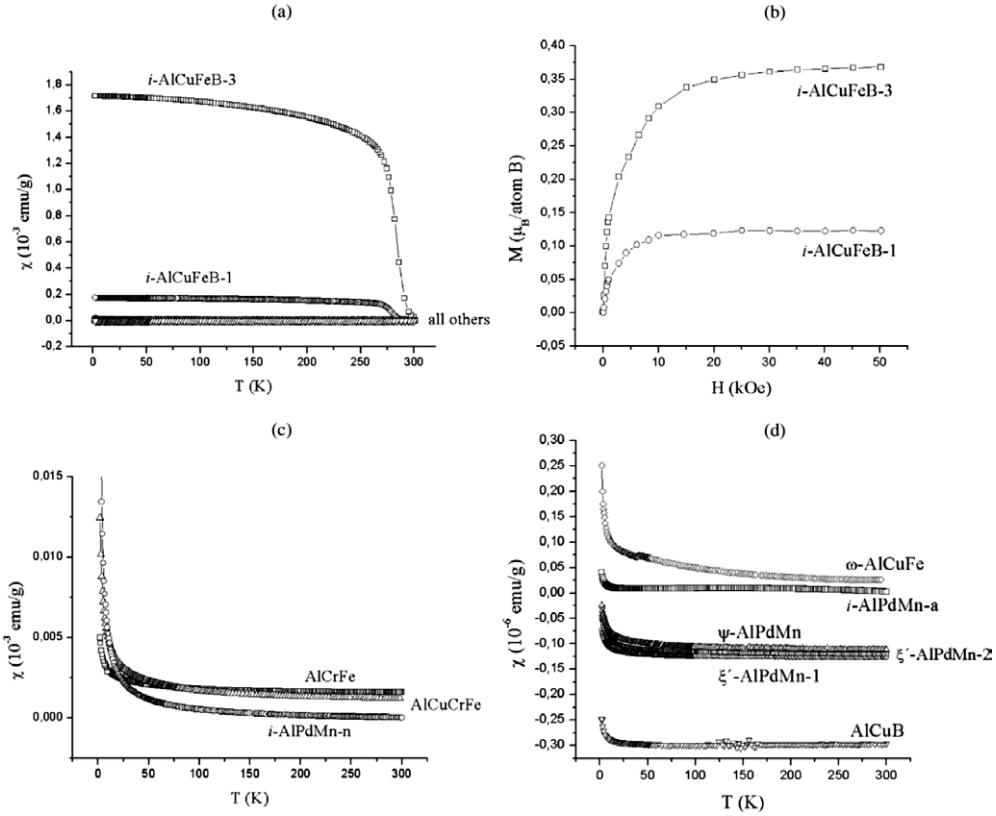

Figure 1. Temperature-dependent magnetic susceptibility χ. (a) Susceptibilities of the two ferromagnetic QC samples i-AlCuFeB-3 and i-AlCuFeB-1 in a field $H = 100$ Oe. The susceptibilities of the other nine samples, measured in a field $H = 1$ kOe, are shown on the same graph in the group 'all others'. (b) Magnetization as a function of the magnetic field at $T = 5$ K for the ferromagnetic samples i-AlCuFeB-3 and i-AlCuFeB-1. (c) Susceptibilities of the paramagnetic samples i-AlPdMn-n, AlCuCrFe and AlCrFe on an expanded vertical scale. (d) Temperature-independent susceptibilities of the samples AlCuB, Ψ-AlPdMn, ξ'-AlPdMn-1, ξ'-AlPdMn-2, ω-AlCuFe and i-AlPdMn-a on a further expanded vertical scale.

upturn below 20 K that originates from the extrinsic magnetic impurities in the samples. The three ξ'-Al–Pd–Mn samples and the AlCuB are diamagnets, exhibiting negative susceptibility in the whole investigated temperature interval, whereas susceptibilities of the ω-AlCuFe and i-AlPdMn-a samples are only slightly positive. It is interesting to compare the magnetism of the two icosahedral samples—the annealed i-AlPdMn-a and the not-annealed i-AlPdMn-n—that were cut from the same ingot, but subjected to different thermal treatment. While the not-annealed sample is a relatively strong Curie paramagnet, this paramagnetism is not present in the annealed sample. Such behaviour is in agreement with previous investigations of the i-Al–Pd–Mn QC family, supporting the conclusion that annealing of the samples improves their quasicrystalline structure and drives their magnetic state towards diamagnetism.

Here we mention that though magnetism is not directly related to the main focus of this study—the electronic DOS, magnetic characterization of the samples was performed due to the fact that localized magnetic moments in significant quantities may influence both the electrical resistivity and the NMR spin–lattice relaxation, which are the techniques used in the following for an indirect determination of the electronic DOS.

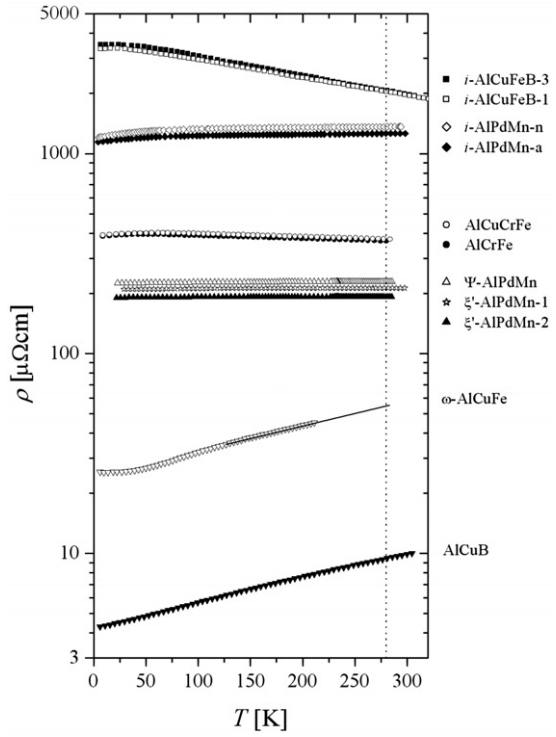

Figure 2. Electrical resistivities of the investigated samples. The vertical dashed line indicates the temperature 280 K, where the resistivity values $\rho_{280\ \mathrm{K}}$ were taken for the correlation analysis.

4. Electrical resistivity

The electrical resistivity was determined in the temperature interval between room temperature (RT) and 4 K using the standard four-terminal technique. The resistivities $\rho(T)$ of all samples are displayed in figure 2. The regular alloy AlCuB exhibits the smallest resistivity within the investigated temperature interval, with ρ values in the range 4–10 $\mu\Omega$ cm (and the RT value $\rho_{280\ \mathrm{K}} = 9.4\ \mu\Omega$ cm). Such ρ values are characteristic of simple alloys. $\rho(T)$ exhibits positive temperature coefficient (PTC) and the resistivity increase from 4 to 280 K is by a factor $(\rho_{280\ \mathrm{K}} - \rho_{4\ \mathrm{K}})/\rho_{4\ \mathrm{K}} = 120\%$. The ω-AlCuFe exhibits slightly larger resistivity (ρ in the range 26–50 $\mu\Omega$ cm with an extrapolated value $\rho_{280\ \mathrm{K}} = 54\ \mu\Omega$ cm). These ρ values are again within the range characteristic of simple alloys. The $\rho(T)$ dependence of ω-AlCuFe is very similar to that of AlCuB, exhibiting PTC and practically the same resistivity increase, $(\rho_{280\ \mathrm{K}} - \rho_{4\ \mathrm{K}})/\rho_{4\ \mathrm{K}} \approx 120\%$ (where the extrapolated RT value was used). The resistivities of the three large-unit-cell ξ'-Al–Pd–Mn samples are one order of magnitude larger than those of regular alloys AlCuB and ω-AlCuFe. Their RT resistivities are $\rho_{280\ \mathrm{K}} = 192\ \mu\Omega$ cm for the ξ'-AlPdMn-2 sample, $\rho_{280\ \mathrm{K}} = 213\ \mu\Omega$ cm for the ξ'-AlPdMn-1 and $\rho_{280\ \mathrm{K}} = 229\ \mu\Omega$ cm for the Ψ-AlPdMn. The remarkable fact is the very small temperature variations of the resistivity for all three samples: the $\rho(T)$ change from 4 to 280 K is $(\rho_{280\ \mathrm{K}} - \rho_{4\ \mathrm{K}})/\rho_{4\ \mathrm{K}} = 0.5\%$ for the ξ'-AlPdMn-2 sample, 1.4% for the ξ'-AlPdMn-1 and 1.7% for the Ψ-AlPdMn. These resistivities can be considered as almost temperature independent. The samples AlCrFe and AlCuCrFe, which are O_1-orthorhombic approximants of the decagonal phase, exhibit still higher resistivities. Their RT values are $\rho_{280\ \mathrm{K}} = 370\ \mu\Omega$ cm for the AlCrFe and

Table 2. Electrical resistivity values at 280 K and the parameter a of the NMR spin–lattice relaxation rate with the calculated DOS reduction factor g_0/g_0(Al) relative to fcc Al metal.

Number	Sample	$\rho_{280\ \mathrm{K}}$ ($\mu\Omega$ cm)	a ($\mathrm{K}^{-1}\ \mathrm{s}^{-1}$)	g_0/g_0(Al) (%)
1	i-AlCuFeB-3	2070	0.0021	6.3
2	i-AlCuFeB-1	2070	0.0021	6.3
3	i-AlPdMn-n	1360	0.016	17
4	i-AlPdMn-a	1260	0.017	18
5	AlCuCrFe	376	0.033	25
6	AlCrFe	370	0.031	24
7	Ψ-AlPdMn	229		
8	ξ'-AlPdMn-1	213		
9	ξ'-AlPdMn-2	192		
10	ω-AlCuFe	54	0.032	25
11	AlCuB	9.4	0.125	49

$\rho_{280\ \mathrm{K}} = 376\ \mu\Omega$ cm for the AlCuCrFe. The $\rho(T)$ values of these two samples already exhibit tiny negative temperature coefficient (NTC), but the increase from 280 to 4 K is small, $(\rho_{4\ \mathrm{K}} - \rho_{280\ \mathrm{K}})/\rho_{280\ \mathrm{K}} = 7\%$ in both cases. The resistivities of the two icosahedral samples i-AlPdMn-a and i-AlPdMn-n are still higher, $\rho_{280\ \mathrm{K}} = 1260\ \mu\Omega$ cm and $\rho_{280\ \mathrm{K}} = 1360\ \mu\Omega$ cm, respectively. Although one of these samples was annealed and the other is as-grown, their resistivity values differ only insignificantly (the not-annealed sample even shows slightly larger resistivity than the annealed one, a feature that is in contrast to the common opinion that annealing drives QCs towards higher resistivity), and their temperature dependence is very weak with a tiny PTC. Finally, the two boron-containing icosahedral QCs, i-AlCuFeB-3 and i-AlCuFeB-1, exhibit the largest RT resistivities of $\rho_{280\ \mathrm{K}} = 2070\ \mu\Omega$ cm in both cases, and a quite significant NTC with the resistivity increase $(\rho_{4\ \mathrm{K}} - \rho_{280\ \mathrm{K}})/\rho_{280\ \mathrm{K}} = 70\%$. The RT resistivity values of the investigated samples are also collected in table 2.

The above resistivities show the following regularity. The resistivities of the two regular alloys (AlCuB and ω-AlCuFe) are low, in the range 10 $\mu\Omega$ cm, with a significant PTC. The three large-unit-cell ξ'-Al–Pd–Mn samples exhibit temperature-compensated (practically zero-temperature-coefficient) resistivities with values of about 200 $\mu\Omega$ cm. The resistivities of the two samples in the decagonal approximant phase (AlCuCrFe and AlCrFe) are still higher (about 370 $\mu\Omega$ cm at RT), but the temperature coefficient has changed sign; there is already a slight NTC. For the two icosahedral i-AlCuFeB-3 and i-AlCuFeB-1 QCs, which exhibit the highest resistivity (of about 2000 $\mu\Omega$ cm at RT), NTC is the strongest. The above results show that low-resistivity samples exhibit pronounced PTCs, whereas increasing resistivity of the samples is accompanied by gradual transformation of the temperature coefficient from positive to negative. For the samples with the RT resistivity of about 200 $\mu\Omega$ cm, the temperature coefficient is essentially zero. The two icosahedral samples i-AlPdMn-a and i-AlPdMn-n are somewhat exceptional regarding their temperature coefficient. While their absolute resistivity values of about 1300 $\mu\Omega$ cm are typical for single-grain i-Al–Pd–Mn QCs, this family of QCs is known to exhibit usually a maximum [12, 13] in the resistivity somewhere between RT and 4 K, which is theoretically still not well understood [14]. In the i-AlPdMn-a and i-AlPdMn-n samples, the maximum has not been observed in the investigated temperature range.

In order to get some microscopic insight into the above empirically determined correlation, we consider, in a qualitative picture, the electrical conductivity ($\sigma = 1/\rho$) to be given by Einstein's formula, valid for a spherical Fermi surface

$$\sigma = e^2 D g(E_\mathrm{F}). \tag{1}$$

Here D is the electronic diffusion constant and $g(E_F)$ is the density of states (DOS) of conduction electrons at the Fermi energy E_F. Within this model, the conductivity is proportional to the product $Dg(E_F)$. In a periodic metallic system, σ is large because $g(E_F)$ is large and, in the absence of structural disorder, the diffusion constant is large as well. In a material without translational periodicity (disordered metals and QCs), σ can be small (or, equivalently, the resistivity $\rho = 1/\sigma$ can be large) due to small $g(E_F)$, but it can be small even if $g(E_F)$ is large, due to the very short mean free path of the conduction electrons (small D). Here it is important to emphasize that equation (1) is applicable to regular metals and alloys and cannot be used directly for the disordered systems and QCs. However, recent theories of electronic transport in QCs [15, 16] consider the conductivity to be still proportional to both D and $g(E_F)$, but quantum interference effects (QIEs) modify the electronic diffusivity D by a weak localization effect (WL) and also induce changes into the DOS function $g(E_F)$ via the electron–electron interactions (EEIs). Depending on the spin–orbit coupling, QIEs can result in increased or decreased resistivity and also affect its temperature coefficient. In the following we shall consider σ to be a function of $g(E_F)$ and make experimental correlation analysis with the $g(E_F)$ values determined on the same set of samples by two other techniques, the NMR spin–lattice relaxation and the soft x-ray emission spectroscopy (SXES). Here it is important to keep in mind that since D is also likely to vary between different samples this can cause uncontrolled errors in such comparisons.

5. Determination of $g(E_F)$ from NMR spin–lattice relaxation

Another technique that is sensitive to the electronic DOS $g(E_F)$ in a metallic system is the NMR spin–lattice relaxation rate T_1^{-1}, where nuclear spins are relaxed via conduction electrons. The conduction-electron relaxation rate T_1^{-1} is written as [17, 18]

$$\frac{1}{\beta_s T_1} = g_0^2 k_B T + g_0 g_0'' \frac{\pi^2}{3}(k_B T)^3. \tag{2}$$

Here $g_0 = g(E_F)$, $g_0'' = (\partial^2 g/\partial E^2)_{E_F}$ is the second derivative of the DOS at the Fermi energy, $\beta_s = (64/9)\pi^3\hbar^3\gamma_e^2\gamma_n^2\langle|u_k(0)|^2\rangle_{E_F}^2$ is the proportionality constant, γ_e and γ_n are the electron and the nuclear gyromagnetic ratios and $\langle|u_k(0)|^2\rangle_{E_F}$ is the density of the electronic wavefunction at the nucleus averaged over the Fermi surface. The linear-in-T term in equation (2) represents the usual Korringa-metallic relaxation, whereas the T^3 term originates from the variation of the DOS ($g_0'' \neq 0$) with energy in the vicinity of E_F. Such variation is present in systems like QCs, where a pseudogap in the DOS at E_F is formed, but is usually absent in regular metals and alloys. Equation (2) is derived for the case where the Fermi contact interaction between conduction s-electron spins and the nuclear spins dominates spin–lattice relaxation. This contribution is usually very dominant in metallic samples where at least a fraction of the conduction electrons exhibit s character.

The analysis of the conduction-electron relaxation rate T_1^{-1} is best performed in the form of a $(T_1T)^{-1}$ versus T plot, which yields for regular metals a horizontal $(T_1T)^{-1} =$ constant line. For that purpose it is convenient to rewrite equation (2) as

$$\frac{1}{T_1T} = a + bT^2, \tag{3}$$

where $a = \beta_s k_B g_0^2$ and $b = \beta_s g_0 g_0''(\pi^2/3)k_B^3$. In our experiment we have performed measurements of the ^{27}Al spin–lattice relaxation rate (as Al is the abundant element in all the investigated samples). In order to extract g_0 from the experimental a value, one should know independently the value of the constant β_s. One may, however, obtain an estimate for g_0

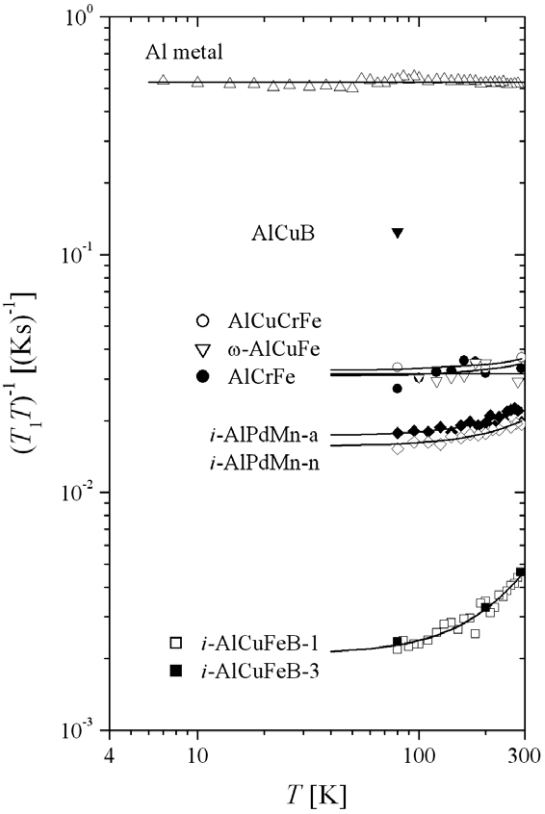

Figure 3. Temperature-dependent ^{27}Al NMR relaxation rates in a $(T_1T)^{-1}$ versus T plot. The relaxation rate of the Al fcc metal (99.999% purity) is shown for comparison.

without explicit knowledge of β_s by normalizing g_0 to the DOS of the fcc aluminium metal, g_0(Al). Pure aluminium is a free-electron-like metal and its NMR relaxation rate exhibits Korringa law $(T_1T)_{Al} = 1.88$ K s [19]. The reduction of g_0 with respect to the DOS of metallic Al is obtained from $g_0/g_0(\mathrm{Al}) = \sqrt{a(T_1T)_{Al}}$, where $(T_1T)^{-1}_{Al} = \beta_s k_B g_0^2(\mathrm{Al})$ and we adopted the approximation that the proportionality constant β_s is the same for the metallic Al and for all other investigated samples.

The ^{27}Al NMR spin–lattice relaxation experiments were performed in the temperature interval from RT to 77 K at the resonance frequency $\nu_0(^{27}\mathrm{Al}) = 26.134$ MHz. The measurements were performed on the central $(1/2 \leftrightarrow -1/2)$ nuclear spin transition of the ^{27}Al (spin $I = 5/2$) nucleus. The saturation-recovery pulse sequence was employed with a saturation train of 60 $\pi/2$ pulses of 2 μs duration. The spin–lattice relaxation rate T_1^{-1} was extracted from the magnetization-recovery curves by the long-saturation magnetic relaxation model of Narath [20], except for the samples of cubic symmetry, where a simple monoexponential recovery was assumed.

The temperature-dependent ^{27}Al NMR relaxation rates are displayed in figure 3 in a $(T_1T)^{-1}$ versus T plot and the relaxation rate of the Al fcc metal (99.999% purity) is shown for comparison. The data were fitted with equation (3) (solid lines), so that the coefficients a could be extracted. Comparing the data of different samples, the following features can be observed in the $(T_1T)^{-1}$ absolute values and their temperature dependence. The samples

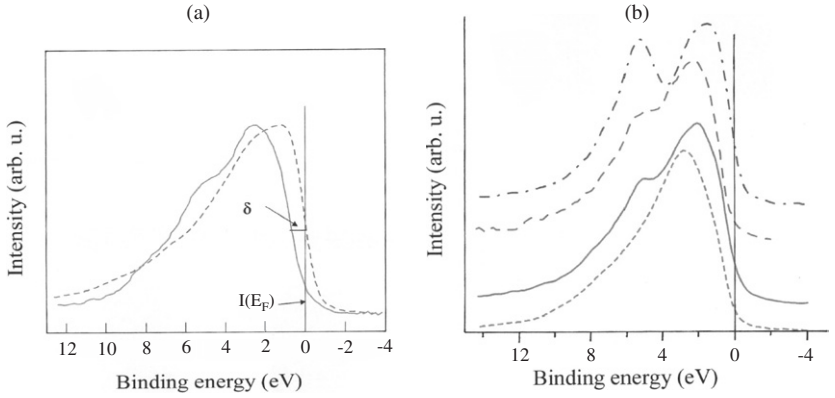

Figure 4. (a) SXES Al 3p spectral curves of fcc Al (dashed line) and icosahedral *i*-Al–Cu–Fe QC (solid line). The relevant parameters are the intensity at the Fermi level, $I(E_F)$, which in fcc Al amounts half the maximum intensity, and the distance δ of the inflection point of the Al 3p edge with respect to E_F, which is zero in fcc Al. The lower the intensity at E_F and the larger the δ, the less metallic is the specimen. (b) SXES Al 3p spectral curves of the samples AlCrFe (dashed line), *i*-AlCuFeB-3 (solid line), *i*-AlPdMn-a (long dash) and AlCuB (dash–dot). For clarity the curves are displaced on the vertical axis.

with increasingly smaller $(T_1T)^{-1}$ values exhibit increasingly larger bT^2 term (observed as a curvature of the $(T_1T)^{-1}$ data above 100 K). The smaller absolute $(T_1T)^{-1}$ value reflects smaller $g_0 = g(E_F)$, whereas the increasing bT^2 term means increasingly stronger variation of the DOS in the vicinity of E_F. Both features are consistent with the existence of a pseudogap in the DOS at E_F, which is most pronounced in the icosahedral QC compounds. The fit-obtained values of the parameter a and the DOS at E_F reduction factors $g_0/g_0(\mathrm{Al}) = \sqrt{a(T_1T)_{\mathrm{Al}}}$ are given in table 2. For the AlCuB simple compound, the DOS reduction factor is 50%, whereas the DOS of the two icosahedral *i*-AlCuFeB samples is reduced to 6% of the fcc Al metal.

6. Determination of DOS by soft x-ray emission spectroscopy

Soft x-ray emission spectroscopy (SXES) is another experimental technique that is suitable to study the electronic DOS. SXES supplies information on the energy distribution of selected partial densities of occupied states around a chosen element in a solid. No absolute densities of states can be obtained, but changes in the electronic structure from one sample to another are detected through changes in the shapes of their partial densities of states. Therefore, only comparison of the same spectral curves from one sample to another makes sense. In Al-containing compounds, the investigation of Al 3p states is particularly interesting, as these states are obtained alone by the SXES technique, so that meaningful comparison with 3p spectral distribution in pure fcc Al is straightforward. Two parameters can be defined in the SXES spectra, as shown in figure 4(a). One is the intensity at the Fermi level, $I(E_F)$, which in pure fcc Al amounts to half the maximum intensity, whereas the other is the distance δ of the inflection point of the Al 3p edge with respect to E_F, which is zero in fcc Al. The lower the intensity at E_F and the larger the δ, the less metallic is the specimen.

In numerous previous investigations [21–24] of Al-based intermetallic compounds with various atomic structures, we have demonstrated that, by comparing to pure fcc Al, $I(E_F)$ in the Al 3p distribution taken at RT varies like the RT electrical resistivity of the sample. Hence, the study of the Al 3p sub-band provides an indication of how free-electron-like a compound

Table 3. Parameters $I(E_F)$ and δ of the Al 3p partial DOS, as obtained from the SXES analysis.

		Al 3p (fcc Al: $I(E_F) = 50$)		Al 3s, d (fcc Al: $I(E_F) \approx 40$)	
Number	Sample	$I(E_F)$ ± 2	δ $\pm 0.1_0$	$I(E_F)$ ± 2	δ $\pm 0.1_0$
1	*i*-AlCuFeB-3	10	0.9	9	0.8
2	*i*-AlCuFeB-1	10	0.8	10	0.8
3	*i*-AlPdMn-n	11	0.7	8	0.9
4	*i*-AlPdMn-a	10	0.8	9	0.8
5	AlCuCrFe	16	0.7_5	17	0.5
6	AlCrFe	15	0.8	9	0.7_5
7	Ψ-AlPdMn				
8	ξ'-AlPdMn-1	19	0.5_5	17	0.5
9	ξ'-AlPdMn-2	19	0.5_5	18	0.4_7
10	ω-AlCuFe	16	0.6	11	0.6
11	AlCuB	35	0.3	32	0.3

may be. Similar conclusions can be derived from the investigation of Al 3s, d states, although in that case difficulties arise from the presence of d-like states near the Fermi level that may strongly interact with transition elements in the compound.

We performed a systematic analysis of the SXES spectra of the same set of samples as used in the electrical resistivity and NMR relaxation experiments, by measuring the Al 3p partial DOS, from which we derive both $I(E_F)$ and δ. The Al 3p spectral curves of some of the investigated samples are displayed in figure 4(b), whereas the $I(E_F)$ and δ parameter values are given in table 3, where the data appear from top to bottom in the order of increasing metallic character. We have verified that the same trend is also followed in the Al 3s, d distributions. The correlation of the SXES results from table 3 with those obtained by the electrical resistivity and NMR relaxation techniques (table 2) is discussed in the next section.

7. Correlation analysis

It is interesting to consider the correlation between the DOS parameters obtained on the same set of samples by the three independent experimental techniques by making an empirical correlation analysis. We recall first the essential information on the DOS obtained from each experiment. The NMR relaxation and SXES techniques yield the relative DOS information, i.e. the reduction of the DOS with respect to pure fcc Al metal. The SXES technique measures the reduction of the Al 3p partial DOS, whereas the NMR relaxation rate is predominantly determined by the s-character electrons via the Fermi contact interaction (as the s-type electrons extend inside the atomic nucleus). If the electronic structure of a solid contains pure s band the NMR relaxation will be predominantly determined by the s electrons, whereas in the case of hybridized sp orbitals both kinds of electrons will contribute significantly to the relaxation rate. The NMR relaxation rate yields, therefore, the reduction of the partial s (or sp) DOS with respect to Al metal, so that the SXES and NMR techniques are in principle sensitive to the same partial character of the DOS. In figure 5 we show the correlation between the $g_0/g_0(\mathrm{Al})$ values from the NMR relaxation experiment and the intensity at the Fermi level $I(E_F)$ of the Al 3p partial DOS obtained by the SXES technique. We observe a linear correlation between the two parameters (the slope of the straight line in figure 5 is $k = 0.9 \pm 0.1$, which confirms a direct one-to-one correlation between $g_0/g_0(\mathrm{Al})$ and $I(E_F)$), with the exception of the two

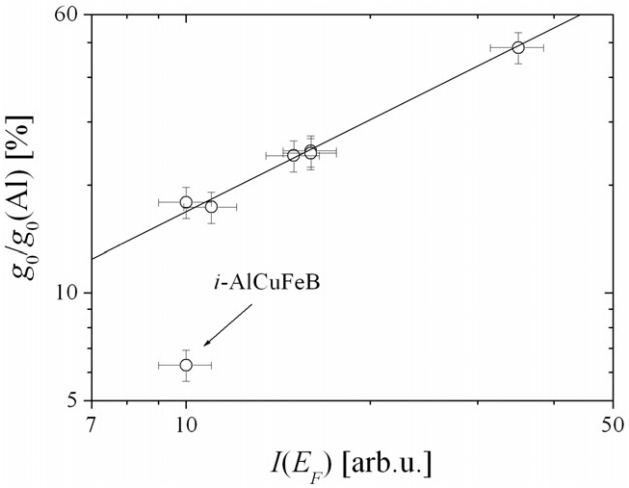

Figure 5. Correlation plot between the g_0/g_0(Al) parameter obtained from the NMR relaxation measurements and the intensity at the Fermi level $I(E_F)$ of the Al 3p partial DOS obtained by the SXES technique. The slope of the straight line is $k = 0.9 \pm 0.1$.

FM QC samples *i*-AlCuFeB-1 and *i*-AlCuFeB-3 that fall out of this correlation. The reason for this exception is not clear; it may be due to ferromagnetism of these two samples, induced by the Fe_2AlB_2 precipitates. The empirical g_0/g_0(Al) versus $I(E_F)$ correlation analysis hence suggests that the NMR relaxation and SXES techniques both 'see' the same reduction of the (partial) DOS at E_F relative to the Al metal.

The electrical resistivity ρ depends on the total DOS at the Fermi energy. For simple metals and alloys one can anticipate equation (1) to hold, implying $\rho \propto 1/g(E_F)$, whereas Mott's theory [25] for systems characterized by the pseudogap in the DOS across the Fermi level yields an inverse-square dependence of the residual ($T \to 0$) resistivity ρ on the DOS, $\rho \propto (g(E_F)/g(E_F)^{free})^{-2}$, where $g(E_F)^{free}$ is the free-electron value. Mizutani [26] has demonstrated empirically that for many icosahedral QC families (with the exception of *i*-Al–Pd–Re) this inverse-square dependence holds at room temperature. In order to see the correlation between the RT resistivity and the DOS parameters g_0/g_0(Al) and $I(E_F)$ of our samples in the sense of [26], we display in figure 6 $\rho_{280\ K}$ versus g_0/g_0(Al), whereas in figure 7 we give $\rho_{280\ K}$ versus $I(E_F)$. In both cases we observe consistently that samples with smaller $I(E_F)$ and g_0/g_0(Al) (less metallic samples) are associated with larger resistivity. In view of the very different conductivity mechanisms in the selected set of samples (as reflected in their different $\rho(T)$ dependences in figure 2), a more quantitative analysis of this empirical result does not appear straightforward.

8. Conclusions

We performed an experimental investigation of the electronic DOS by three independent experimental techniques: electrical resistivity, NMR spin–lattice relaxation and SXES. The investigated set of 11 samples contained aluminium as the majority constituent element and included transition elements Cu, Fe, Cr, Pd and Mn, whereas B was added to some samples in small concentration for an improved mechanical strength. Magnetic measurements have shown a variety of magnetic states—diamagnetism, paramagnetism and ferromagnetism.

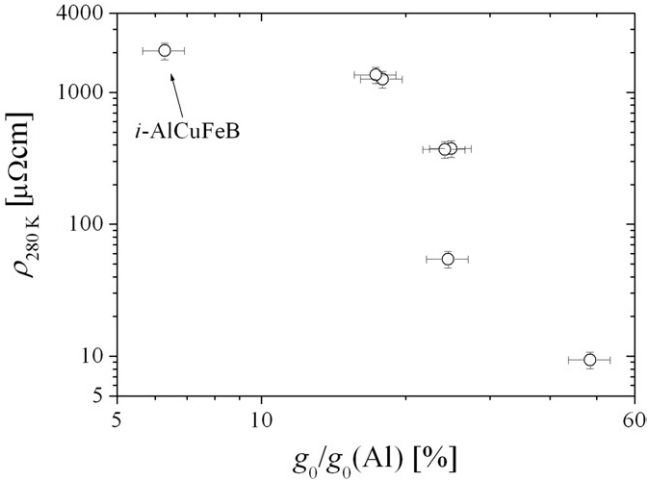

Figure 6. Correlation plot of the RT electrical resistivity $\rho_{280\,K}$ against g_0/g_0(Al), determined from the NMR relaxation, for the investigated set of samples.

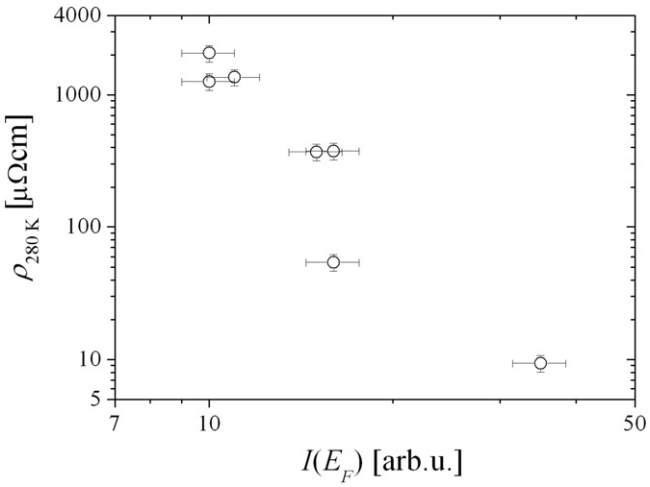

Figure 7. Correlation plot between the RT electrical resistivity $\rho_{280\,K}$ and the parameter $I(E_F)$ of the Al 3p partial DOS.

Ferromagnetism was observed in the two icosahedral *i*-AlCuFeB QCs, where its origin (ferromagnetic Fe_2AlB_2 precipitates) is extrinsic to the icosahedral state. The DOS of the selected samples was determined indirectly via measurements of the electrical resistivity and the ^{27}Al NMR spin–lattice relaxation rate, whereas SXES allowed for a direct determination of the Al 3p partial DOS. Correlation analysis between the DOS parameters obtained by the three techniques showed that the order of samples with decreasing metallic character was the same in all experiments, where the more resistive samples show smaller DOS at the Fermi level. Quantitative evaluation of the DOS at E_F has shown that in simple alloys the DOS is reduced to about 50% of the free-electron-like value in fcc Al, whereas the reduction is increasingly larger on going to large-unit-cell periodic solids with coexisting large-scale periodicity and atomic-scale quasiperiodic orders and finally to icosahedral quasicrystals without translational

periodicity. Our results also demonstrate that low resistivities are accompanied with PTC variations, whereas in samples with large resistivity the variation becomes NTC. Samples with the resistivity of about 200 $\mu\Omega$ cm appear to be at a crossover from PTC to NTC resistivity, resulting in a temperature-compensated resistivity with essentially zero temperature coefficient. This result, obtained here on purely experimental grounds, points towards the possibility of 'compositional tuning' of the resistivity, that might be of interest in technological applications. Our investigation of the DOS in a large variety of samples may also provide a basis for the investigation of wetting of oxidized metallic surfaces by polar liquids, where the molecules of a liquid are considered to interact electrostatically with the conduction electron cloud within the bulk metallic material.

Acknowledgments

This work was done within the 5th Framework EU project 'Smart quasicrystals' (contract No G5RD-CT-2001-00584). We are especially grateful to M C de Weerd and V Khare (Nancy) and M Feuerbacher (Juelich) for the provision of the samples and A Smontara (Zagreb) for performing electrical resistivity measurements.

References

[1] Dubois J M, Fournée V and Belin-Ferré E 2004 *Quasicrystals 2003—Preparation, Properties and Applications* (*Mat. Res. Soc. Symp. Proc.* vol 805) ed E Belin-Ferré, M Feuerbacher, Y Ishii and D J Sordelet, p 287
[2] See, e.g., Janot C 1994 *Quasicrystals* (Oxford: Clarendon) p 372
[3] See, e.g., Abragam A 1961 *The Principles of Nuclear Magnetism* (Oxford: Oxford University Press) p 358
[4] Belin-Ferré E 2001 *J. Phys.: Condens. Matter* **13** R1
[5] Brien V, Khare V, Herbst F, Weisbecker P, Ledeuil J B, de Weerd M C and Dubois J M 2005 *J. Mater. Res.* at press
[6] Dong C and Dubois J M 1991 *J. Mater. Sci.* **26** 1647
[7] Demange V, Ghanbaja J, Beeli C, Machizaud F and Dubois J M 2004 *J. Mater. Res.* **19** 2285
[8] See, for a review, Feuerbacher M, Thomas C and Urban K 2003 *Quasicrystals, Structure and Physical Properties* ed H-R Trebin (Weinheim: Wiley–VCH) p 2
[9] Boudard M, Klein H, de Boissieu M, Audier M and Vincent H 1996 *Phil. Mag.* A **74** 939
[10] Klein H, Audier M, Boudard M, de Boissieu M, Behara L and Duneau M 1996 *Phil. Mag.* A **73** 309
[11] Behara L, Duneau M, Klein H and Audier M 1997 *Phil. Mag.* A **76** 587
[12] Akiyama H, Hashimoto T, Shibuya T, Edagawa K and Takeuchi S 1993 *J. Phys. Soc. Japan* **62** 939
[13] Lanco P, Klein T, Berger C, Cyrot-Lackmann F, Fourcaudot G and Sulpice A 1992 *Europhys. Lett.* **18** 227
[14] Dolinšek J, Klanjšek M, Jagličić Z, Bilušić A and Smontara A 2002 *J. Phys.: Condens. Matter* **14** 6975
[15] Rapp Ö 1999 *Physical Properties of Quasicrystals* ed Z M Stadnik (New York: Springer) p 127
[16] Fujiwara T 1999 *Physical Properties of Quasicrystals* ed Z M Stadnik (New York: Springer) p 169
[17] Hill E A, Chang T C, Wu Y, Poon S J, Pierce F S and Stadnik Z M 1994 *Phys. Rev.* B **49** 8615
[18] Dolinšek J, Klanjšek M, Apih T, Smontara A, Lasjaunias J C, Dubois J M and Poon S J 2000 *Phys. Rev.* B **62** 8862
[19] Spokas J J and Slichter C P 1959 *Phys. Rev.* **113** 1462
[20] Narath A 1967 *Phys. Rev.* **162** 320
[21] Belin-Ferré E and Dubois J M 1996 *J. Phys.: Condens. Matter* **8** L717
[22] Belin-Ferré E 1999 *Quasicrystals* (*Mater. Res. Soc. Symp. Proc.* vol 553) ed J M Dubois, P A Thiel, A P Tsai and K Urban, p 347
[23] Belin-Ferré E, Fournée V and Dubois J M 2000 *J. Phys.: Condens. Matter* **12** 8159
[24] Belin-Ferré E 2002 *J. Phys.: Condens. Matter* **14** R789
[25] Mott N F 1969 *Phil. Mag.* **19** 835
[26] Mizutani U 1998 *J. Phys.: Condens. Matter* **10** 4609